SAND2013-4674C

Fault Analysis of Plasma Facing Component Mounts Using Multiphysics Simulation

D.L. Youchison, J.D. Kotulski, and M.A. Ulrickson
Sandia National Laboratories, Albuquerque, NM USA
dlyouch@sandia.gov

***Abstract*—Plasma facing components like the ITER blanket shield modules (BSMs) often consist of a first wall and a shield block that are mounted to a vacuum vessel wall. The ITER mount is comprised of an Inconel bolt, Ni-Al-bronze collar, insulating layers of alumina and a flexible Inconel cartridge that allows compliance to reduce stress. Here we describe our efforts to perform multiphysics simulations on the flexible mount using current densities calculated for ITER halo scenarios and off-normal disruption events over various size faults or breaks in the insulator layers. This effort also entailed a study of fault size and simulations of high current flow over small area faults that would likely lead to melting. In addition to ohmic heating and thermal analysis, melting and solidification physics were included using computational fluid dynamics to track the solid/liquid interface and the degree of melting near the fault. Temperature dependent conductivities were used for the solid and liquid phases of all the materials. We concluded that for the anticipated off-normal conditions in ITER, the flexible mount is very fault tolerant for both large and small area faults.**

Keywords—fault, mounts, plasma facing component, blanket shield module, computational fluid dynamics, multiphysics, melting, solidification

I. INTRODUCTION

The ITER blanket shield modules (BSM's) are attached to the first wall using flexible mounts. These mounts must react the large forces and torques that occur during off-normal plasma events such as disruptions and also allow the modules to move and reduce stress. Both eddy currents and halo currents can flow through the flexible mounts if the alumina insulating layers fault. In addition to creating large forces and torques, the ohmic heating at the fault location may result in melting or destruction of the Inconel or aluminum bronze flexible mount components.

The flexible mounts are a critical component since they position and secure the BSMs in relation to the ITER plasma. Fig. 1 shows the geometry of a flexible mount. It consists of an Inconel bolt and nut, a nickel aluminum bronze (UNS C63200) collar and an Inconel centering cone, and a flexible cartridge also made of Inconel. All the Inconel is Inconel-718. The device connects the shield block to the vacuum vessel through a nickel aluminum bronze collar. The bolt is insulated from the collar by a thick alumina insulating layer on the cone and from the Inconel cartridge by an alumina layer deposited on the top mating surface of the cartridge. Two other alumina layers protect the nut. The compliance is provided by a flexible cartridge that allows the mount to bend and twist under applied electromagnetic loads.

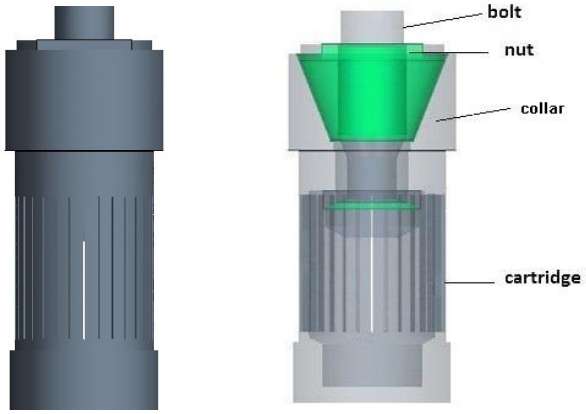

Fig. 1. Flexible mount geometry. Insulators are shown in green.

We first investigated the effects of eddy currents generated by plasma disruptions on faults of various sizes at the insulating layer on the conical nut of the flexible mount. Following this, we developed a simple 3D model of a small fault similar to a fuse link as shown in Fig. 2. It consists of an Inconel cylinder 1-cm in diameter attached to an aluminum nickel bronze cylinder of the same size through a 1-mm-DIA fault section. The purpose of the small fault model was to discover the excitation or maximum current density that could be tolerated in a small fault that did not lead to destruction of the main mount bodies. Both eddy and halo current loads were evaluated.

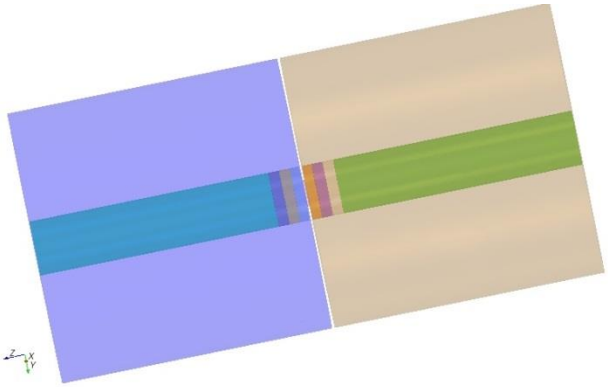

Fig. 2. Cross section through the simple small fault. Ni-Al-bronze on right.

Sandia is a multiprogram laboratory managed and operated by Sandia Corporation, a wholly owned subsidiary of Lockheed Martin Corporation, for the United States Department of Energy's National Nuclear Security Administration under contract DE-AC04-94AL85000.

II. MULTIPHYSICS MODELS

A. Disruption Case

A commercial multiphysics code, Star CCM+ version 8.02, was used for the fault analysis [1]. CCM+ was also able to include the localized volumetric power generation from ohmic heating and capture the phase transformations during melting and solidification. We included a volume-of-fluid capability in the physics model to track the solid/liquid interface in the bronze and Inconel, but not the alumina.

Various magnitudes of constant potential or excitation were applied to the outside face of the collar and the bottom face of the cartridge. Transient analysis was performed to determine the current density distribution in the geometry. The simulation spanned 200 ms using time steps of 0.5 ms and 10 inner iterations per time step. Temperature and phase dependent conductivities were used for the Inconel and nickel-aluminum bronze. The specific heats and densities are constants. The volume fraction of liquid produced by melting provided a measure of damage for later comparison.

First, a 30^o sector of the conical alumina insulator was faulted by applying a constant electrical conductivity of copper ($6.0x10^7$ S/m) to that sector, while retaining the thermal conductivity of alumina (20 W/mK). We applied a uniform voltage of 1.0V on the outside of the bronze collar for a 30 ms pulse as shown in Fig. 3. Secondly the size of the fault was increased to a 90^o sector. And finally, to the 90^o sector fault, we added a fault encompassing the entire alumina annulus under the collar.

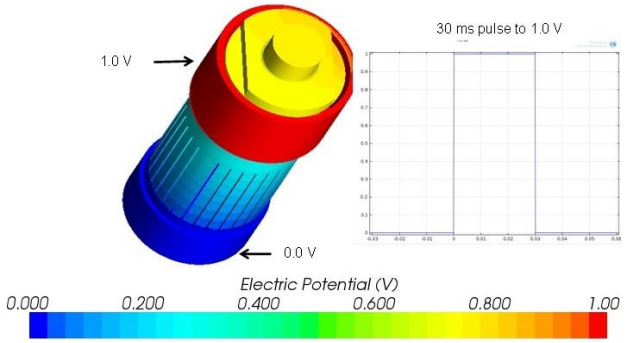

Fig. 3. Potential distribution with faulted conical insulator at 20 ms. Inset shows 30 ms voltage pulse.

For the second and third cases, we input the current density distribution as a function of time during the worst case 40 ms downward linear vertical displacement event [2] disruption on BSM-01 as calculated in Opera-3d ELEKTRA [3] using input from the DINA code for the disruption history [4]. The current density fit is shown in Fig. 4. The simulation was performed to 100 ms to relax the temperature distribution. At the end of the disruption, the current density is 1.0E6 A/m^2 corresponding to an applied potential of 0.12 V.

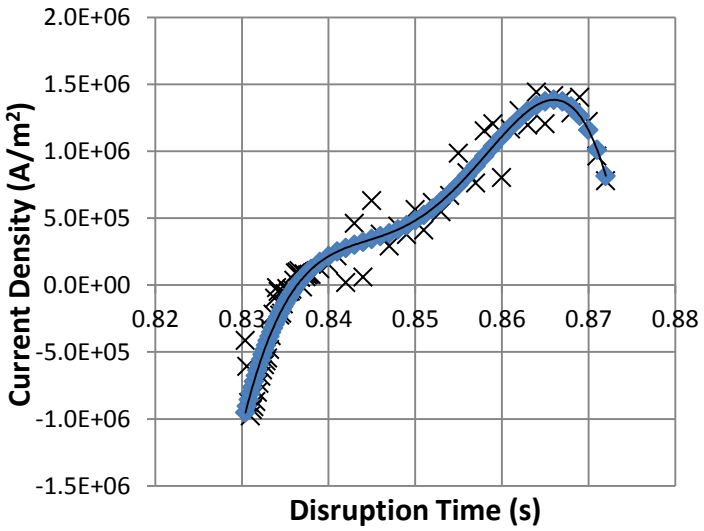

Fig. 4. ITER downward linear vertical displacement event transient current density taken from Opera-3d results.

Although larger size faults may appear to be a worse case, the current density distribution through the fault may actually be smaller and not produce much ohmic heating. However, smaller area faults will have a higher current density for the same excitation compared to larger faults and will produce much higher localized heating.

The simplified small fault geometry shown in Fig. 2, consisting of a 1-cm-dia Inconel-718 cylinder joined to a 1-cm-dia nickel aluminum bronze cylinder by a 1-mm-dia alumina insulator, 100 microns thick, was faulted in the same manner as the flexible mount insulators.. The current densities through the fault are quite high resulting in intense ohmic heating near the fault and melting of the adjacent materials. The simulation was run to 30 ms using the normalized disruption profile from the linear downward vertical displacement event case with the peak adjusted to 1, 2 and 4 V.

B. Halo Current Case

Halo currents can also drive faults in insulators. In most cases the halo currents are smaller than disruption currents, but can last ten times longer. In this case, we performed simulations on only the small fault model, since it should see the largest effect. The predicted halo current through BSM-01 has a linear triangular waveform shown in Fig. 5 that rises during the first 108.8 ms and falls during the last 161.8 ms for a total duration of 207.6 ms. The peak was set to 0.40 V and 0.75 V, respectively for the two most probable excitation conditions.

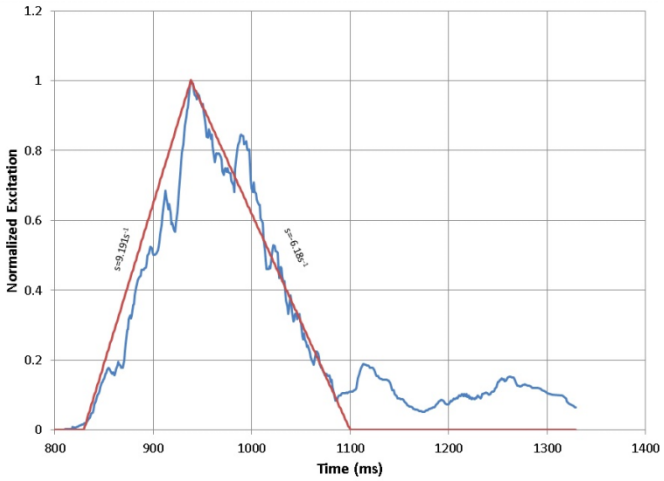

Fig. 5. Fit to predicted halo current in first wall of BSM-01.

C. *Meshing*

The mesh for the 3D flexible mount model consisted of 498k polyhedral cells. The mesh was refined at the fault areas on the alumina insulators. The mesh appears in Fig. 6 below. Three prism layers in the mesh are adjacent to the outer surfaces to better define the current densities near the surfaces.

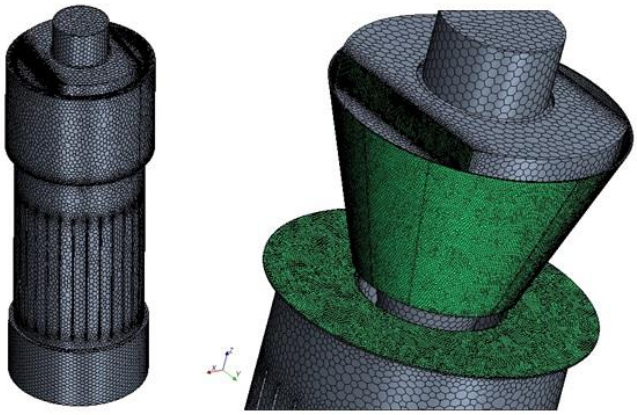

Fig. 6. 498 k cell polyhedral mesh (left) with close-up of 90° fault zone and faulted disk layer (right).

The mesh for the small fault model was heavily refined at the fault. It consisted of 64.9k polyhedral cells as shown in Fig. 7. The 5-cm-dia outer volumes are not shown for clarity. Boundary conditions included keeping the entire face of the far Inconel end at 0.0 V and applying constant positive excitations for 30 ms to the entire face of the far bronze end. Constant excitations of 1, 2, 3 and 4 V were applied to the bronze end.

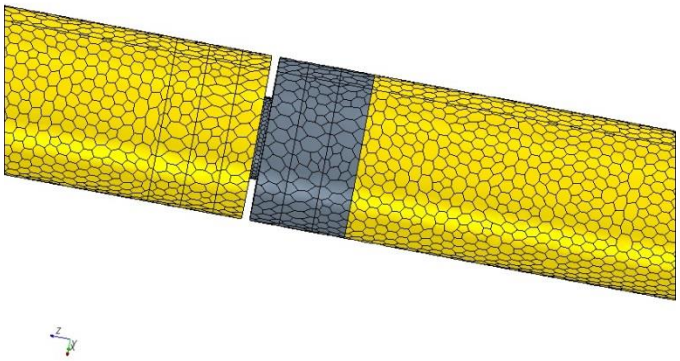

Fig. 7. Mesh shows the refined zone at the fault in the center of the view.

The analysis used both temperature and phase dependent properties for the electrical and thermal conductivities of Inconel-718 and the Ni-Al-Bronze [5-7]. These are shown in Fig. 8and Fig. 9 for the bronze and Inconel, respectively. We used a constant density of Inconel of 8000 kg/m^3 and a specific heat of 435.5 J/kgK. For the bronze, we used a density of 7600 kg/m^3 and a specific heat of 439 J/kgK. The bronze heat of fusion is 219.3 kJ/kg with a liquidus temperature of 1363 K and a solidus temperature of 1343 K. Energy absorbed by the heat of fusion reduces the temperature in the bronze parts. The melting points of the bronze and the Inconel are 1090 °C and 1337 °C, respectively. We used a constant dynamic viscosity of 0.0037 Pa-S for the liquid bronze. The small fault had a thermal conductivity of 20 W/mK, with a constant density of 8940 kg/m^3, an electrical conductivity of 5.96E7 S/m, and a specific heat of 386 J/kgK.

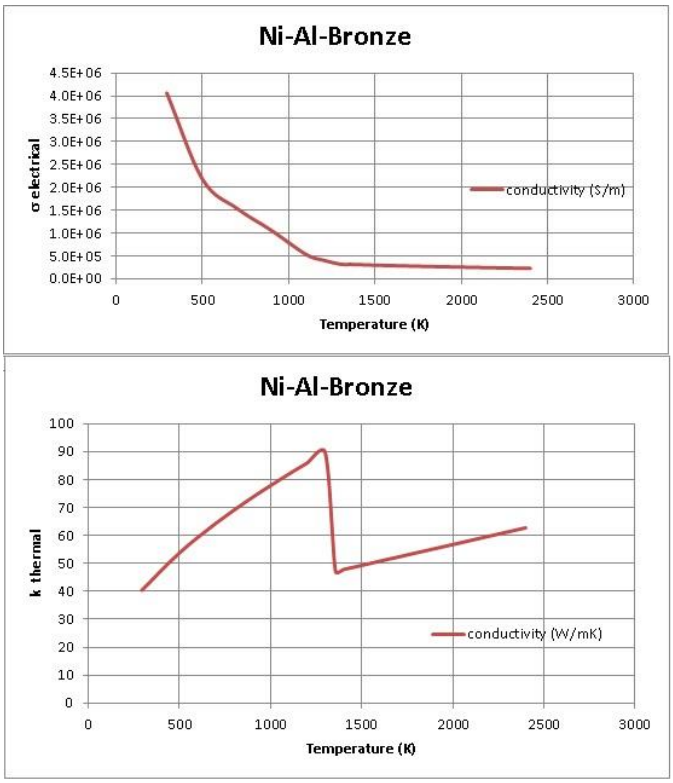

Fig. 8. Ni-Al-Bronze conductivities

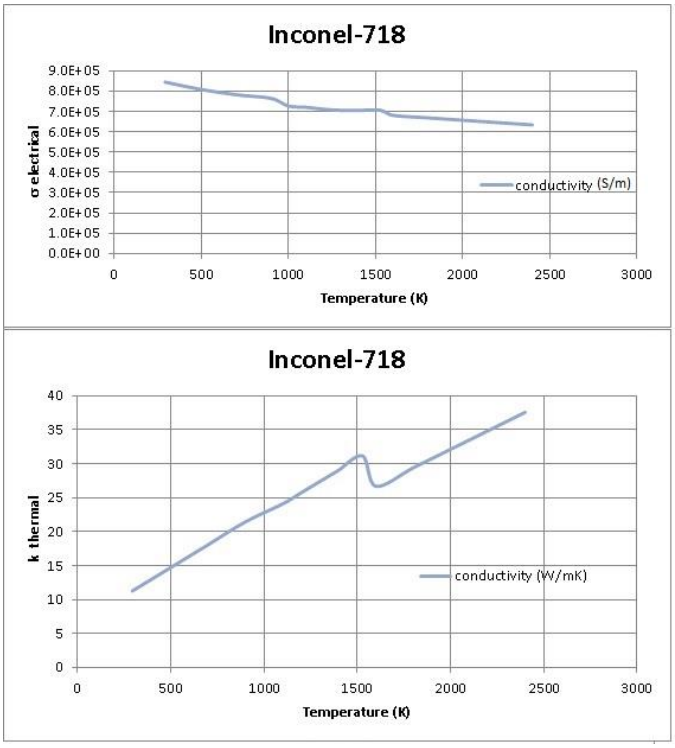

Fig. 9. Inconel-718 conductivities

III. RESULTS

Results for the flexible mount with a 30 ms constant excitation on a 30° fault of the conical insulator appear first, followed by the 90° fault combined with a full fault on the alumina layer under the collar. The results for the small fault appear next for the downward vertical displacement disruption (VDE) scaled to 1, 2 and 4 V. Finally, we present the results on the small fault for the triangular halo current profile scaled to the 0.4 and 0.75V maximums.

A. Disruption Eddy Currents

The current density distribution in the middle of the 30 ms pulse appears in Fig. 10 for the 30° sector fault in the conical insulator. The current densities in the Inconel cartridge are low. The temperature distribution at 200 ms from the start of the 30 ms pulse shows localized edge effects and appears in Fig. 11. The maximum temperature increase is approximately 60 °C which would not be detrimental to the bolt or mount.

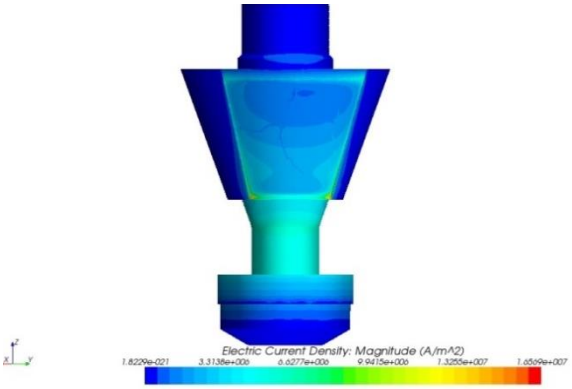

Fig. 10. Current density distribution at t=20 ms for a 30° fault.

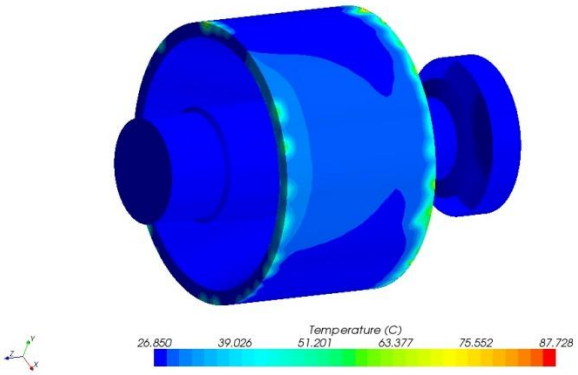

Fig. 11. Temperature distribution in bronze collar and Inconel bolt at 200 ms.

The current density distribution for the combined 90° conical and annular insulator fault at 40 ms appears in Fig. 12. This simulation uses the absolute VDE current densities obtained from Opera-3d as shown in Fig. 4. The temperature increase is negligible. Therefore, even the large fault would not be detrimental to the mount.

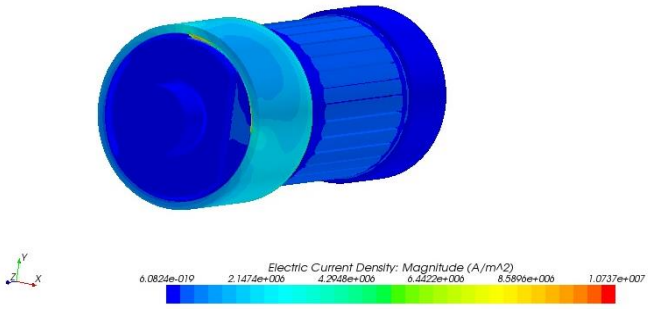

Fig. 12. Current densities are modest for the down linear vertical displacement disruption at t=40 ms.

Next, we investigated a small fault using the shape of the downward linear vertical displacement event, but with four very large peak values of 1, 2, 3 and 4 V. The temperature distribution and solid fraction for the small fault with the 4 V peak appear in the axial cutplane shown in Fig. 13 and Fig. 14, respectively. For these high excitation cases, there is very little radiation loss due to the internal geometry; however, the heat of vaporization was neglected. Its inclusion would result in slightly lower temperatures near the melt zone and a reduction in the liquid fraction, but would not change the solid fraction. The melting proceeds radially and axially along a spherical front following the temperature contours. The current density increases from an average value near 6.4E09 A/m^2 in the bronze near the fault for the 1V case to nearly 2.1E10 A/m^2 for the 4 V case. All the cases are summarized in Table I.

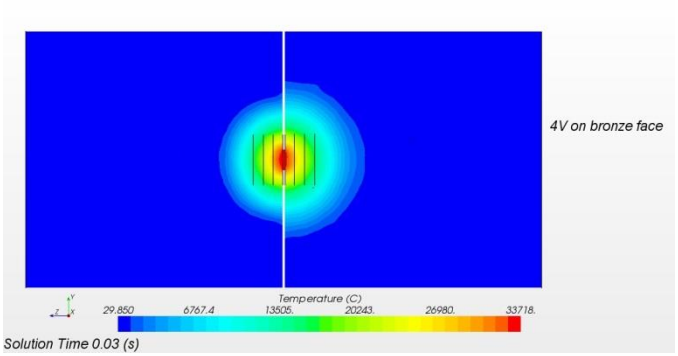

Fig. 13. Temperature distribution for 4 V peak excitation at 30 ms.

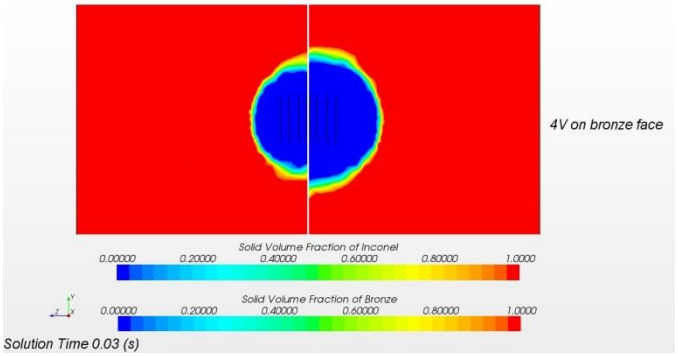

Fig. 14. Solid fraction for 4 V peak excitation at 30 ms.

B. Halo Currents

The 0.4 V peak halo current excitation applied to the small fault resulted in a peak temperature of 1549 ^{o}C and an average current density of 2.6E09 A/m^2. The solid fraction at the peak of the excitation appears in Fig. 15. A very small volume of both the bronze and the Inconel melts, but solidifies before the pulse is over. The combined melt volume is less than 1 mm^3.

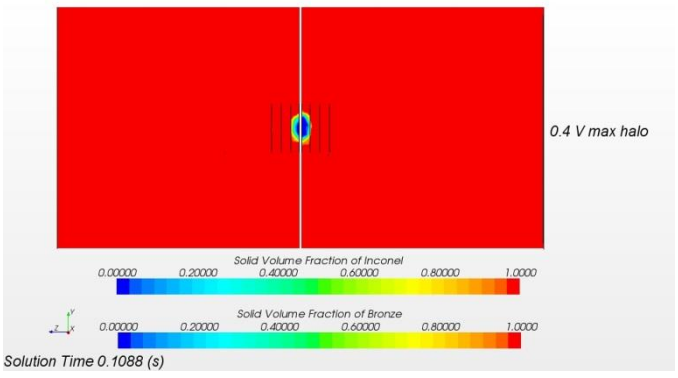

Fig. 15. Solid fraction at the peak of the 0.4 V excitation reveals little melting.

The 0.75 V peak results in more melting of the bronze and Inconel parts, but the melt volumes are smaller than the disruption cases. The temperature distribution at the current peak has a maximum of 4145 ^{o}C as shown in Fig. 16. The solid fraction at the peak is shown in Fig. 17. The fault cools down after the peak and begins to solidify. The solid fraction at the end of the pulse, t=0.2706 s, appears in Fig. 18. The results are summarized in Table II below.

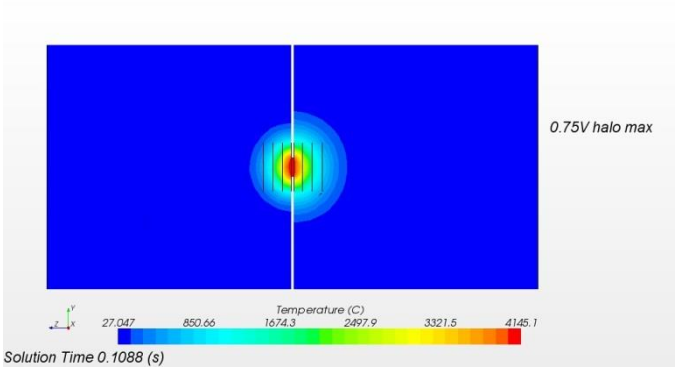

Fig. 16. Peak temperature distribution caused by 0.75V peak excitation.

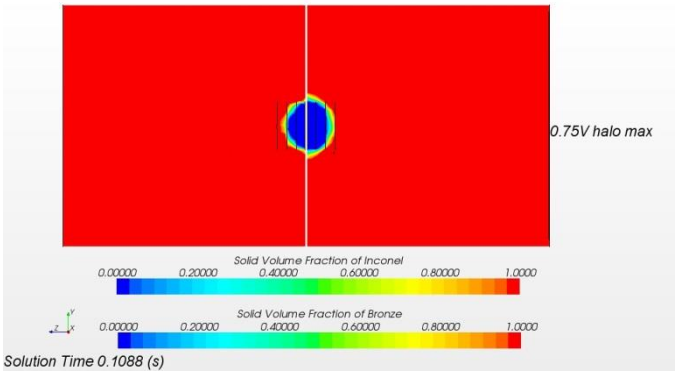

Fig. 17. Solid fraction at t=0.1088 s, the peak of the 0.75 V excitation.

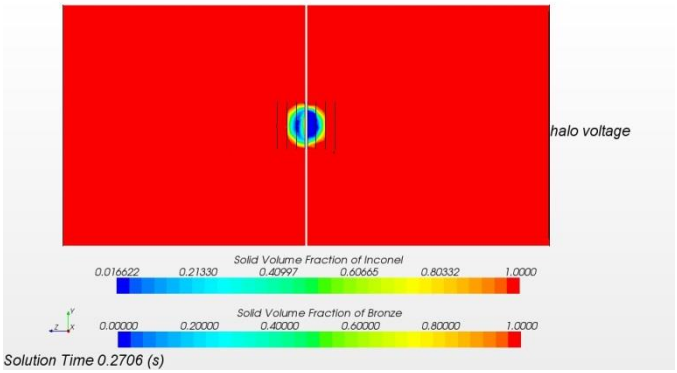

Fig. 18. Solid fraction at the end of the 0.75 V excitation pulse, t=0.2706 s.

TABLE I. SMALL FAULT – 30 ms DISRUPTION EXCITATION

Voltage	Contact Area	Max. Temperature	Joule Heat	Average Current Density[a]	Intensity	Bronze Melt Volume	Inconel Melt Volume
[V]	*[mm^2]*	*[^{o}C]*	*[W]*	*[A/m^2]*	*[A]*	*[mm^3]*	*[mm^3]*
1.0	0.785	6382	6.08E03	6.4E09	6.08E03	5.46	3.03
2.0	0.785	15289	2.44E04	1.3E10	1.22E04	19.41	10.35
3.0	0.785	24549	5.49E04	1.8E10	1.83E04	36.37	19.14
4.0	0.785	33980	9.72E04	2.1E10	2.43E04	56.65	28.70

a. Local average centered in front of the fault

TABLE II. SMALL FAULT – 270 ms HALO EXCITATION

Voltage	Contact Area	Max. Temperature	Joule Heat	Average Current Density[b]	Intensity	Bronze Melt Volume	Inconel Melt Volume
[V]	*[mm^2]*	*[^{o}C]*	*[W]*	*[A/m^2]*	*[A]*	*[mm^3]*	*[mm^3]*
0.40	0.785	1549	9.72E02	2.6E09	2.43E03	0.37	0.24
0.75	0.785	4145	3.42E03	4.8E09	4.56E03	3.03	1.90

b. Local average centered in front of the fault

IV. CONCLUSION

Large area faults in the conical insulator and the annular insulating layer at the bottom of the collar do not result in any melting in the flexible mount. This is particularly true for the current density distribution predicted from previous Opera-3d runs. Only very small faults where the current density is much higher produce localized melting.

A small fault, 1 mm in diameter, was modeled in a simple 0.1 mm thick alumina junction between Ni-Al-bronze and Inconel 718. A 2 V, 30 ms excitation, which created a peak current density of $3.9X10^{10}$ A/m^2 (3-4 orders of magnitude higher than that expected for a disruption), produced only localized melting in the radial center of the bronze part closest to the fault. Such a melt zone would rapidly re-solidify after the disruption by thermal conduction into the bulk mass. Higher excitations of 3V and 4 V resulted in larger melt zones during the 30 ms duration. As mentioned earlier, results from Opera-3d simulations reveal that current densities from a 2V excitation used in the small fault simulations are well above that predicted for ITER disruptions.

The expected worst case halo current through the first wall of BSM-01 caused by a 270 ms triangular excitation with a 0.75 V peak produced very little melting in the bronze. This would not cause significant damage to a small fault. However, additional runs showed that significant melting and even vaporization will occur above 2.0 V.

If one neglects MHD effects, we can conclude that the current insulator design for the flexible mount is very fault tolerant for both small and large faults during ITER transients. However, if large volumes of melt layer are removed and not contained by the surrounding solid volumes, the damaged volume of the mount will expand with each passing disruption.

ACKNOWLEDGMENT

The authors wish to thank James Bullock for model CAD support. The views and opinions expressed herein do not necessarily reflect those of the ITER Organization.

REFERENCES

[1] *Star-CCM+ version 8.02.008 User Guide*, CD-adapco, Inc., New York, 2012.

[2] J.D. Kotulski, R.S. Coats and M.F. Pasik, "Electromagnetic Analysis of Transient Forces Due to Disrupted Plasma Currents on the ITER Shield Modules," Proc. IEEE/NPSS 22nd Symp. on Fusion Engr., 2007

[3] *Opera-3d version 15 User Guide*, Vector Fields Limited, England, 2012.

[4] R.R. Khayrutdinov and V.E. Lukash, " Studies of Plasma Equilibrium and Transport in a Tokamak Fusion Device with the Inverse-Variable Technique," *J. Comp. Physics*, **109** 193-201, 1993.

[5] P.J. Macken and A.A. Smith, *The Aluminum Bronzes, Properties and Production Processes*, Copper Development Association, publication No. 31, 2nd edition, St. Albans, UK, 1966

[6] G. Pottlacher, H. Hosaeus, E. Kaschnitz, and A. Seifter, "Thermophysical Properties of Solid and Liquid Inconel 718 Alloy", *Scandinavian Journal of Metallurgy*, **31** 161-168, 2002.

[7] V. Barabash, "Summary of Material Properties for Structural Analysis of the ITER Internal Components," ITER_D_23HL7T v. 3.2, 2009..